# Simple and Accurate Determination of Reactivity Ratios Using a Nonterminal Model of Chain Copolymerization

Bryan S. Beckingham,[†] Gabriel E. Sanoja,[†,‡] and Nathaniel A. Lynd[*,†,§]

[†]Joint Center for Artificial Photosynthesis, Materials Sciences Division, Lawrence Berkeley National Laboratory, Berkeley, California 94720, United States

[‡]Department of Chemical and Biomolecular Engineering, University of California, Berkeley, California 94720, United States

[§]McKetta Department of Chemical Engineering, University of Texas at Austin, Austin, Texas 78712, United States

S Supporting Information

ABSTRACT: We propose a new method for the determination of reactivity ratios based on a nonterminal model of copolymerization kinetics. Within the context of this model, we derive simple, reactivity-ratio-dependent expressions whose solution relies solely on monomer consumption information spanning the full range of conversion. Utilizing this method, reactivity ratios are obtained for the aluminum chelate-catalyzed copolymerization of phenyl glycidyl ether and allyl glycidyl ether ($r_{PGE} = 1.56 \pm 0.01$ and $r_{AGE} = 0.66 \pm 0.03$) with monomer consumption monitored by *in situ* ^{1}H NMR spectroscopy. Additionally, this approach is applied to experimental data extracted from the literature for other copolymerization systems encompassing a range of monomer types (styrenics, isoprene, lactones, lactide, and other cyclic ethers) and polymerization type (anionic, coordination, and zwitterionic) to obtain reactivity ratios under the mechanistic assumption of nonterminal model copolymerization kinetics. We present the nonterminal model of copolymerization as the first method that should be utilized before more complex frameworks (e.g., terminal or penultimate model of chain copolymerization) are used to understand copolymerization kinetics.
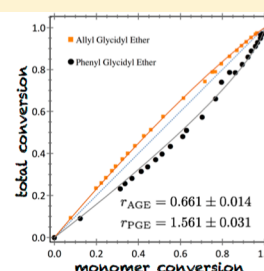
Non-terminal reaction kinetics for IDEAL Copolymerizations

$$\sim\!\!\sim\!\!\sim^* \; + \; A \; \xrightarrow{k_A} \; \sim\!\!\sim\!\!\sim\!A^*$$

$$\sim\!\!\sim\!\!\sim^* \; + \; B \; \xrightarrow{k_B} \; \sim\!\!\sim\!\!\sim\!B^*$$
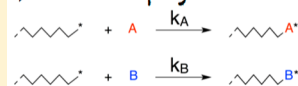
Allows facile determination of reactivity ratios

$$P_{AB}(p_A) = 1 - n_A\left(\frac{A(t)}{A_0}\right) - (1 - n_A)\left(\frac{A(t)}{A_0}\right)^{r_B}$$

$$P_{AB}(p_B) = 1 - n_A\left(\frac{B(t)}{B_0}\right)^{r_A} - (1 - n_A)\left(\frac{B(t)}{B_0}\right)$$

$r_{AGE} = 0.661 \pm 0.014$
$r_{PGE} = 1.561 \pm 0.031$

INTRODUCTION

The ability to synthesize tailored polymers with specified functionalities and physical properties is fundamental to understanding and ultimately controlling structure−property relationships. Over the past several decades, there have been significant advances in the synthesis and characterization of such polymer materials. In this context, chain copolymerization—the simultaneous polymerization of multiple monomers—is an important strategy to synthesize polymers with desirable physical properties. Through statistical control over the distribution of monomers along the polymer chain, a wide variety of sequence distributions can be achieved with consequently varying and tunable physical properties.[1−8] Therefore, understanding the statistics of monomer addition to the propagating chain end is critical both in elucidating structure−property relationships as a function of copolymer composition and microstructure, and in developing high-performance materials.[4,7−11]

The instantaneous copolymer composition (i.e., compositional drift) of a chain copolymerization has been traditionally described using a terminal model of copolymerization.[12−14] The model assumes the chemical reactivity of the propagating chain to depend on the identity of the repeat unit at the growing end and neglects the preceding chain composition as shown in Figure 1a. If we consider the copolymerization of two monomers A and B (Figure 1a) within the terminal model, four

distinct propagation rate constants (k_{AA}, k_{AB}, k_{BB}, k_{BA}) describe the incorporation of monomer into the growing polymer chain. Here, k_{AB} is the binary propagation rate constant for the reaction between a propagating chain ending in A and adding monomer B, and so on. The reactivity ratios r_A and r_B can be understood as the tendency of the propagating chain end species to self-propagate and enchain its own type of monomer over that of the other monomer. As the reactivity ratios are thereby a representation of the compositional drift that results from the difference in monomer reactivity during the copolymerization, they are commonly used to discern between the four well-established types of copolymerization behavior (gradient, random, alternating, and blocky) as depicted in Figure 1b.[14]

The elementary chemical reactions presented in Figure 1a, together with the initiation steps, can be used to generate a system of coupled ordinary differential equations (ODEs) describing the kinetics of chain copolymerization (eqs 1 and 2). Here, $A(t)$, $B(t)$, and $X(t)$ are the respective time-dependent concentrations of A monomer, B monomer, and X initiator; $A^*(t)$ and $B^*(t)$ are the time-dependent concentrations of polymer chains with A and B units as their terminal species, and

(a)

(b)

ABABABABABABABABABABABAB alternating ($r_A = r_B = 0$)

AAAAABBBBBAAAAABBBBBBAAAAA blocky ($r_A, r_B \gg 1$)

AAAAAAAAAABABBABBBABBBBBBB gradient ($r_A > 1 > r_B$)

ABAABABBABAAABABABBABAABAB random ($r_A = r_B = 1$)

Figure 1. (a) Reactivity ratios are defined by the ratios of the propagation rate constants for adding a monomer (A or B) to a growing chain end of the same identity. $r_A = k_{AA}/k_{AB}$ represents the preference of a chain with a terminal A unit for similar monomers of type A and likewise for r_B. (b) Reactivity ratios (r_A, r_B) describe the statistical incorporation of monomer into a single chain resulting in one of four classical macromolecular regioisomers: alternating, blocky, gradient, or random.

k_{XA} and k_{XB} are the respective rate constants for initiation of A monomer and B monomer:

$$-\frac{dA}{dt} = k_{AA}A(t)A^*(t) + k_{BA}A(t)B^*(t) + k_{XA}A(t)X(t)$$

(1)

$$-\frac{dB}{dt} = k_{BB}B(t)B^*(t) + k_{AB}B(t)A^*(t) + k_{XB}B(t)X(t)$$

(2)

This system of ODEs is nonlinear and cannot be solved analytically, but with a steady-state assumption can be reformulated into the classical copolymer equation used as the basis for nearly all methods of determining reactivity ratios:

$$F_A = \frac{r_A f_A^2 + f_A f_B}{r_A f_A^2 + 2f_A f_B + r_B f_B^2}$$

(3)

Methods based on eq 3 include techniques such as Mayo–Lewis,[13] Fineman–Ross,[15] and Kelen–Tüdős,[16] among other possibilities.[17] Because the underlying ODEs were not integrated, the resultant copolymer equation is a reactivity-ratio-dependent algebraic description of the instantaneous relationship between monomer feed (f_A or f_B) and the resultant copolymer composition (F_A). This expression holds as long as the f_A and f_B remain constant. For any system where r_A and $r_B \neq 1$, eq 3 is only a valid approximation at low monomer conversion. Therefore, all of the aforementioned methods based on eq 3 are also only strictly applicable at low monomer conversion. In general, to determine reactivity ratios, several copolymerizations of varied initial monomer composition (f_A) are initiated and then terminated at low conversion (approximately 5−10%) so that changes in the monomer feed composition are minimal, and finally the resulting copolymer composition is characterized.[18] The results are then interpreted within the context of a specific formulation of eq 3.[13,15,16]

Ideal copolymerizations are those in which the propagating species exhibit the same tendency to react with either monomer. This does not necessitate a random copolymeriza-

tion but merely signifies that the chain ends are generally indiscriminate in their reactivity. Thus, this type of copolymerization behavior requires $k_{AA} = k_{BA}$ and $k_{BB} = k_{AB}$ which implies that the $r_A \times r_B$ product is unity. The comonomers may exhibit differences in reactivity that lead to gradient formation. Note that in the special case where $r_A = r_B = 1$ the monomers show equal reactivity toward the propagating species and will be distributed randomly along the chain. However, this constitutes a special case, and thus a copolymer microstructure should not be assumed to be random without determination of the reactivity ratios for a given monomer pair or demonstration of a uniform composition profile along the polymer chain. As the rates of monomer incorporation in ionic copolymerizations (e.g., anionic, cationic, zwitterionic, and coordination−insertion) generally do not exhibit a strong dependence on the identity of the chain end,[9,14,19] as assumed in the terminal model, and instead are primarily dictated by the chemistry of the monomers, they tend to exhibit *ideal* behavior. This characteristic of ionic and pseudoionic copolymerizations suggests that they can be described with a kinetic model that assumes the reactivity of the propagating species to be independent of the composition of the chain and only depend on the reactivity of the incoming monomer. The mechanistic basis for this statement is that the monomer incorporation statistics are determined by the interaction of an incoming monomer with a cation, anion, or metal center and that the nature of that interaction does not depend on the identity of the last monomer enchained.

Accordingly, we develop a nonterminal model for copolymerization and derive integrated expressions that describe the compositional drift for nonterminal copolymerizations. We validate the model using compositional drift data obtained from the ring-opening polymerization of allyl glycidyl ether and phenyl glycidyl ether monitored by *in situ* ^{1}H NMR spectroscopy and previous reports on copolymerizations of vinyls, lactones, lactides, and other cyclic ether monomers. The method provides a simple and accurate tool for determining the reactivity ratios for systems that can be described using a nonterminal model of copolymerization.

■ EXPERIMENTAL SECTION

Materials. All chemicals were used as received from Sigma-Aldrich unless otherwise specified. All air- and moisture-sensitive reactions were carried out using standard Schlenk-line techniques. Diethyl ether was collected from a commercial J.C. Meyer dry solvent system immediately prior to use. Acetyl acetone was degassed by freeze−pump−thaw (FPT) cycles and vacuum distilled prior to use. DI water was sparged with nitrogen gas for 45 min prior to use. Allyl glycidyl ether and phenyl glycidyl ether were degassed by FPT cycles and distilled from butylmagnesium chloride prior to use. Deuterated ether (*d*-10) was received in a sealed ampule and transferred into a septum-capped vial in an inert nitrogen atmosphere glovebox prior to use.

Instrumentation. ^{1}H NMR spectra were collected on a Bruker Inova Avance 500 MHz spectrometer at room temperature and referenced to the residual nondeuterated solvent shift of diethyl ether (*d*-10).

Vandenberg Catalyst Preparation. The Vandenberg catalyst was prepared on a Schlenk line in a flame-dried and septum-sealed round-bottom flask charged with a Teflon stir bar. Anhydrous diethyl ether (40 mL) and triethylaluminum (1.0 M AlEt$_3$ in hexanes, 40 mL, 40 mmol) were sequentially added with a gastight syringe under 5 psi nitrogen pressure. *Caution! AlEt$_3$ is a pyrophoric and moisture-sensitive material and should be handled with appropriate care.* The reaction mixture was stirred for 30 min and then immersed in an ice bath to cool to 0 °C. Acetyl acetone (2.04 mL, 20 mmol) was then added with
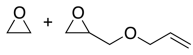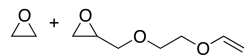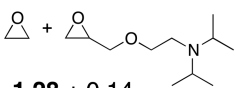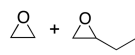
a gastight syringe through the septum. After stirring for 2 h, DI water (0.36 mL, 20 mmol) was added drop-wise with a gastight syringe. The reaction mixture was allowed to stir overnight at room temperature with periodic venting of the produced ethane gas prior use.

Vandenberg-Catalyzed Synthesis of Poly[(allyl glycidyl ether)-co-(phenyl glycidyl ether)]. The polymerization was carried out in a 7 in. thin-walled Wilmad NMR tube fitted with a septum cap. The reaction tube was flame-dried under vacuum followed by backfilling with nitrogen (5 psi) four times. Under positive nitrogen pressure, deuterated ether (d-10), allyl glycidyl ether, and phenyl glycidyl ether were added with a gastight syringe through the septum cap. Prior to polymerization, an initial ^{1}H NMR spectrum was collected to determine the initial monomer composition (69% allyl glycidyl ether and 31% phenyl glycidyl ether). Upon addition of the Vandenberg catalyst (0.25 mL) with a gastight syringe, the tube was immediately returned to the spectrometer, and collection of ^{1}H NMR spectra during the course of the polymerization was started. The monomer consumption was quantified through the epoxide ring C—H: allyl glycidyl ether δ 3.00 (O—CH$_2$—C$\underline{\text{H}}$—CH$_3$) and phenyl glycidyl ether δ 3.18 (O—CH$_2$—C$\underline{\text{H}}$—CH$_3$).

■ RESULTS AND DISCUSSION

Nonterminal (i.e., ideal) copolymerization behavior is expected for ionic and pseudoionic copolymerizations where the rate of monomer incorporation does not exhibit a strong dependence on the identity of the terminal unit but instead is dictated solely by the nature of the reacting monomers. This assertion is supported by previous reports on anionic ring-opening copolymerizations of various epoxides where the product of the reactivity ratios tends toward unity (Table 1)[6,9,18,20,21] but also other ionic copolymerizations.[14,22]

Table 1. Reactivity Ratios of Monosubstituted Epoxides and EO[a]

(a)

r_{EO} = **3.1 ± 0.4**
r_{PO} = **0.30 ± 0.04**

(b)

r_{EO} = **1.20 ± 0.01**
r_{EEGE} = **0.76 ± 0.02**

(c)

r_{AGE} = **1.31 ± 0.26**
r_{EO} = **0.54 ± 0.03**

(d)

r_{EGVGE} = **3.50 ± 0.90**
r_{EO} = **0.32 ± 0.10**

(e)

r_{DEGE} = **1.28 ± 0.14**
r_{EO} = **0.82 ± 0.10**

(f)

r_{EO} = **6.46 ± 0.05**
r_{BO} = **0.148 ± 0.002**

[a](a) PO = propylene oxide,[18] (b) EEGE = ethyl ethoxy glycidyl ether,[20] (c) AGE = allyl glycidyl ether,[9] (d) EGVGE = ethylene glycol vinyl glycidyl ether,[9] (e) DEGE = N,N-diisopropyl ethyl glycidyl amine,[21] and (f) BO = butylene oxide.[6]

Polyethers are an important and versatile class of materials typically synthesized through the ring-opening polymerization (ROP) of epoxide-based monomers, as their physical properties can be controlled through the functional groups attached to the monomers and the copolymerization stoichiometry.[6,9,14,18] Although the driving force for the ROP of epoxides is the strain inherent to the ring—which does not strongly depend on the structure of the pendant substituent—Table 1 contains evidence to justify that ideal behavior (but not random) is generally observed in the ROP of epoxides.[6,9,18,20,21] Therefore, interpretation of the compositional drift of these systems using

the terminal model of copolymerization is not necessarily justified due to a superfluous dependence on chain-end structure that is not justified by experimental observations. We propose that these and related ionic copolymerizations may be more appropriately described using a kinetic model that does not contain the explicit dependence on the identity of the propagating chain end and that a simpler *nonterminal* model of copolymerization may be sufficient.

Derivation of Nonterminal Model for Determination of Reactivity Ratios. A nonterminal model of copolymerization kinetics can be derived to describe the monomer incorporation statistics associated with *ideal* chain copolymerization. The model is based at the outset on the assumption that the chemical reactivity of the propagating chain is independent of polymer composition as shown in Figure 2a.
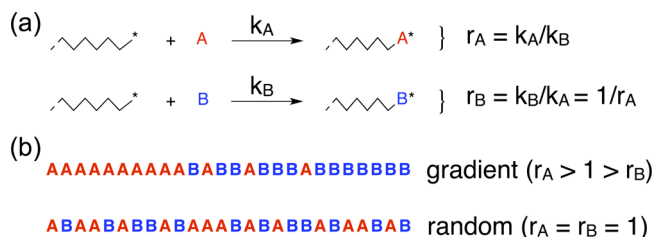
Figure 2. (a) Reactivity ratios are defined by the ratios of the propagation rate constants for adding a monomer (A or B) to a growing chain end of the same identity. $r_A = k_A/k_B$ represents the preference of the A-chain end for similar monomers of type A and likewise r_B. (b) Reactivity ratios (r_A, r_B) describe the statistical incorporation of comonomers into a single chain.

Consequently, only one propagation rate constant is required per monomer, rather than two as used in the terminal model. Analogous to the terminal model of copolymerization kinetics discussed above, the values of the reactivity ratios determine the resulting polymer microstructure and the extent to which monomer enchainment deviates from a statistically random distribution. However, note that the nonterminal model of copolymerization cannot describe alternating and blocky monomer distributions as their formation strongly relies on the chain end reactivity.

The nonterminal model allows the description of the kinetics of chain copolymerization using a system of ODEs (eqs 4−6) based on the elementary reactions presented in Figure 2a together with the initiation steps. For simplicity, k_A and k_B are the respective rate constants for initiation and propagation of A and B, and A_0, B_0, and X_0 are the respective initial concentrations for monomers A and B as well as initiator X. This system of ODEs is the same that would be obtained if eqs 1 and 2 would be rewritten under the assumption of $k_{AA} = k_{BA} = k_A$ and $k_{BB} = k_{AB} = k_B$. This is because the model presented in this paper constitutes a limiting case of the terminal model historically used in the polymer chemistry literature.

$$-\frac{dA}{dt} = k_A A(t)(A^*(t) + B^*(t) + X(t)) = k_A A(t) X_0 \tag{4}$$

$$-\frac{dB}{dt} = k_B B(t)(B^*(t) + B^*(t) + X(t)) = k_B B(t) X_0 \tag{5}$$

$$-\frac{dX}{dt} = [k_A A(t) + k_B B(t)] X(t) \tag{6}$$

The system of ODEs is linear and can be readily integrated analytically using an appropriate set of initial conditions and the assumption of livingness $(X_0 = A^*(T) + B^*(T) + X(T))$ to yield exponentially decaying monomer and initiator concentrations as a function of time (eqs 7–9).

$$A(t) = A_0 e^{-k_A X_0 t} \tag{7}$$

$$B(t) = B_0 e^{-k_B X_0 t} \tag{8}$$

$$X(t) = X_0 e^{(-1/X_0)(A_0 - A(t) + B_0 - B(t))} \tag{9}$$

The time-dependent concentrations of monomers and initiator (eqs 7–9) constitute a system of equations that can be used to relate the reactivity ratios to experimentally observable quantities. Because the underlying ODEs (eqs 4–6) could be integrated over time or conversion, any method of determining reactivity ratios based on this model will not be restricted to low conversion or invariant monomer feed composition. Our interest is primarily in using the experimentally measured compositional drift to determine reactivity ratios. To do this, we write an expression for the total monomer conversion (p_{AB}) as a function of time or conversion (eq 10). Here, n_A and n_B are the initial mole fractions of A and B. The explicit time dependence is eliminated using eqs 7 and 8.

$$
\begin{aligned}
\text{total conversion} &= \frac{A_0 + B_0 - A(t) - B(t)}{A_0 + B_0} \\
&= \frac{A_0 + B_0 - A_0 e^{-k_A X_0 t} - B_0 e^{-k_B X_0 t}}{A_0 + B_0} \\
&= n_A + n_B - n_A e^{-k_A X_0 t} - n_B e^{-k_B X_0 t} \\
&= 1 - n_A \left(\frac{A(t)}{A_0} \right) - n_B \left(\frac{B(t)}{B_0} \right)
\end{aligned}
\tag{10}
$$

Compositional drift data are typically presented as mole fraction of monomer in the copolymer as a function of initial monomer composition; yet in this case it is experimentally more convenient and algebraically simpler to state the problem as total monomer conversion (p_{AB}) as a function of individual monomer conversion. A set of equations that relate the compositional drift of each monomer to the reactivity ratios are derived by substituting $n_B = 1 - n_A$ and inserting the following reactivity-ratio-dependent relations into eq 10:

$$\frac{A(t)}{A_0} = \left(\frac{B(t)}{B_0} \right)^{r_A}$$

$$\left(\frac{A(t)}{A_0} \right)^{r_B} = \frac{B(t)}{B_0} \tag{11}$$

Equations 12 and 13 enable a simple and accurate determination of reactivity ratios at all conversions for copolymerizations that can be described by the nonterminal model of copolymerization kinetics. Here, p_A and p_B are the respective conversions of A and B monomer with $p_A = 1 - (A(t)/A_0)$.

$$p_{AB}(p_A) = 1 - n_A(1 - p_A) - (1 - n_A)(1 - p_A)^{r_B} \tag{12}$$

$$p_{AB}(p_B) = 1 - n_A(1 - p_B)^{r_A} - (1 - n_A)(1 - p_B) \tag{13}$$

^{1}H NMR spectroscopy, or any method that can monitor the composition of monomer as a function of overall conversion, can then be used to determine reactivity ratios based on data spanning the full range of conversion. In particular, the overall monomer conversion (p_{AB}) may be plotted as a function of individual monomer conversions (p_A, p_B) and the resulting data set fit to eqs 12 and 13.

In order to explore the effectiveness of the presented model for determining reactivity ratios, we investigate simulated copolymerization data, the copolymerization of allyl glycidyl ether and phenyl glycidyl ether monitored by *in situ* ^{1}H NMR spectroscopy, and a broad range of copolymerizations with compositional drift data readily available in the literature.

Numerical Validation of Nonterminal Model via Simulated Ideal Copolymerizations. The derived nonterminal model's capacity for fitting the compositional drift of copolymerizations was explored through a series of six simulated *ideal* copolymerizations. The differential equations that describe the classical terminal model (eqs 1 and 2) were numerically integrated using an adaptive fifth-order Runge–Kutta with an error goal of 10^{-12} for prescribed $(r_A = 1.05–3.20)$ and ideal $(r_B = 1/r_A)$ reactivity ratios. Thus, the full kinetic data for monomer consumption were obtained for these reactivity ratios from which compositional drift data were extracted as shown in Figure 3. The nonterminal model could
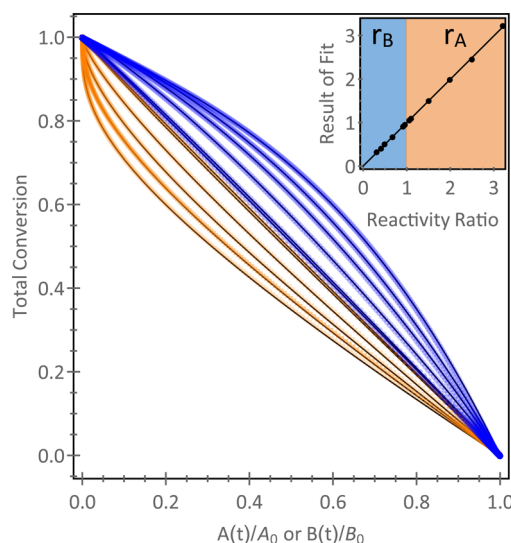
Figure 3. Equations 12 and 13 were systematically evaluated by generating six data sets by numerically integrating (adaptive fifth-order Runge–Kutta with error goal of 10^{-12}) the terminal-model description for an ideal copolymerization with $r_A = 1.05–3.20$ ($r_B = 1/r_A = 0.95–0.31$) and $A_0 = B_0 = 0.5$, $X_0 = 0.01$. The compositional drift results, shown in blue and orange, were extracted from the raw kinetic data and fit (—) to eqs 12 and 13.

then be evaluated by applying it to the terminal model compositional drift for these reactivity ratios and thereby evaluate its ability to reproduce the reactivity ratios.

It is readily apparent, qualitatively, from a visual inspection of Figure 3 that the nonterminal model achieves excellent fits to the simulated compositional drift data. From a quantitative comparison of the prescribed and calculated reactivity ratios (as shown by the inset in Figure 3), we find excellent agreement between the prescribed reactivity ratio and the reactivity ratio

obtained by the nonterminal model as in all cases the nonterminal model was within 2% error of the input value.
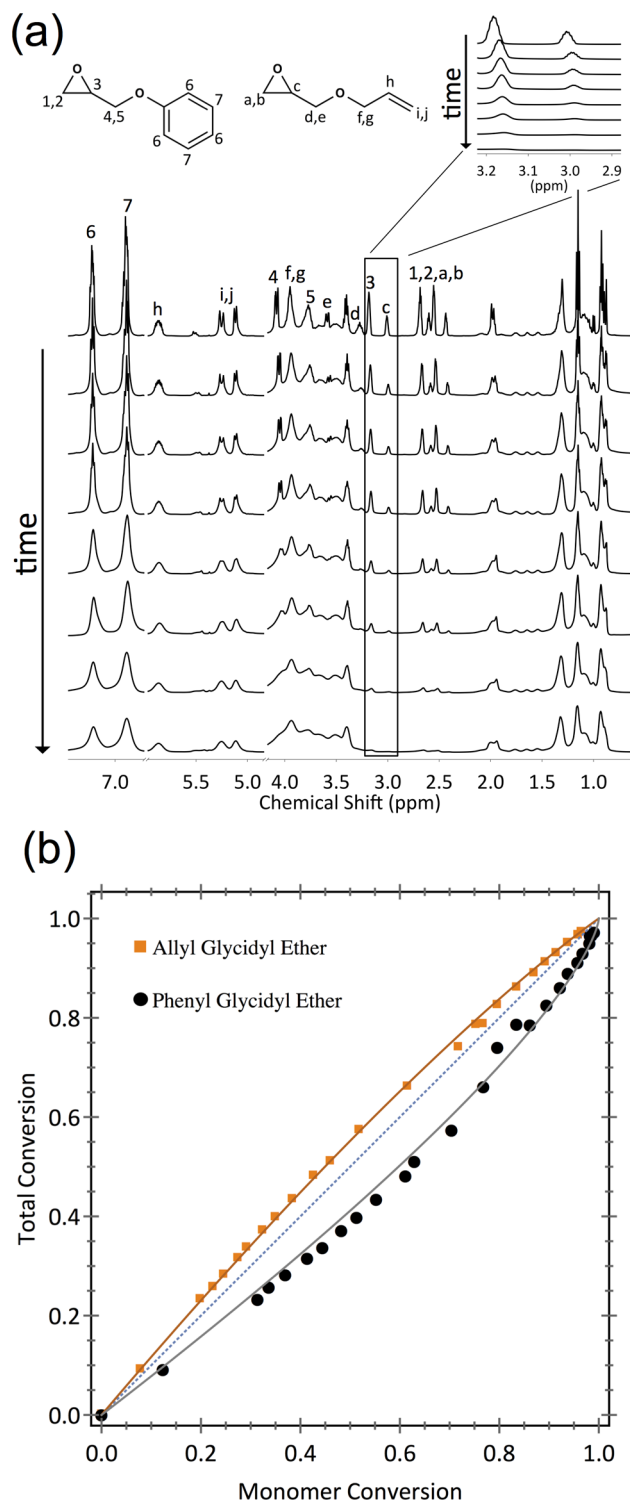
Vandenberg-Catalyzed Copolymerization of Allyl Glycidyl Ether and Phenyl Glycidyl Ether. Having found the nonterminal model capable of determining reactivity ratios with good numerical accuracy with simulated copolymerization data, we next applied the model to the copolymerization of allyl glycidyl ether (AGE) and phenyl glycidyl ether (PGE) using the Vandenberg catalyst.[23] Compositional drift data were obtained using ^{1}H NMR spectroscopy to monitor the polymerization *in situ* allowing the measurement of both monomer conversions and thereby total conversion as a function of time. Figure 4a shows a subset of the ^{1}H NMR spectra obtained in this manner, with the relevant epoxide ring CH signals expanded in the inset on the upper right. As the disappearance of these CH signals corresponds to ring-opening and inclusion of the respective monomers into the growing chain, they are used as a measure of monomer conversion during the course of the polymerization (Figure 4b).

The total conversion as a function of monomer conversion data presented in Figure 4b together with the initial mole fractions of AGE (n_{AGE}) and PGE (n_{PGE}) were fit to eqs 12 and 13 to obtain reactivity ratios for this pair of epoxides; $r_{PGE} = 1.56 \pm 0.01$ and $r_{AGE} = 0.66 \pm 0.03$. Upon visual inspection, the nonterminal model appears able to capture the chemistry of chain copolymerizations across the full span of conversion with excellent overlay between the experimental data and the computed curves (solid orange and gray lines in Figure 4b). In particular, fitting the experimental compositional drift of AGE and PGE yields reactivity ratios whose product tends toward the anticipated copolymerization *ideality* ($r_{PGE} \times r_{AGE} = 1.03 \pm 0.04$). The high quality of the fit of the experimental data with the nonterminal model is reflected quantitatively by the very low standard regression errors obtained (less than 2% of the reactivity ratios).

The application of the nonterminal model to the copolymerization of AGE and PGE here highlights the ease with which monomer conversion data may be obtained and analyzed to determine reactivity ratios that reflect the observed compositional drift. Overall, these qualities make this model a useful initial method for characterizing compositional drift—determining reactivity ratios in particular—in lieu of the more labor-intensive traditional approaches.

Application of Nonterminal Model Reactivity Ratio Equations to Literature Data. Having established the validity and ease of this approach for determining reactivity ratios for simulated data and the AGE/PGE system, we next applied this model to a wide range of copolymerization chemistries for which the requisite compositional drift data was readily available in the literature.[2,24−30] To explore the broad applicability of the model, we chose a wide range of monomers and polymerization type such as the anionic copolymerization of styrene (S) and isoprene (I),[2] the coordination polymerization of L-lactide (L-LAC) and ε-caprolactone (ε-CL),[29] and the zwitterionic copolymerization of ε-caprolactone (ε-CL) and δ-valerolactone (δ-VL).[27] In total, the model was applied to the compositional drift data of nine copolymerizations yielding the model fits shown in Figure 5 with the corresponding reactivity ratios given in Table 2 along with the chemical structures for each copolymerization.

As was observed for the copolymerization of AGE and PGE, the model is able to capture the observed compositional drift for all nine of the systems presented in Figure 5. We focus on

Figure 4. (a) Time-resolved 500 MHz ^{1}H NMR spectra of a Vandenberg-catalyzed copolymerization of allyl glycidyl ether and phenyl glycidyl ether. Inset expands region of interest for observation of the epoxide ring CH signals for allyl glycidyl ether (3.0 ppm) and phenyl glycidyl ether (3.18 ppm) whose integration was utilized to yield the respective monomer conversions. (b) Total polymerization conversion plotted against monomer conversion: (■) allyl glycidyl ether and (●) phenyl glycidyl ether. Solid orange and gray lines represent fits to the experimental data using the nonterminal model, eqs 12 and 13, and the initial compositions: $n_{AGE} = 0.69$ and $n_{PGE} = 0.31$. The dotted blue line represents the random copolymerization case: $r_{AGE} = r_{PGE} = 1$.
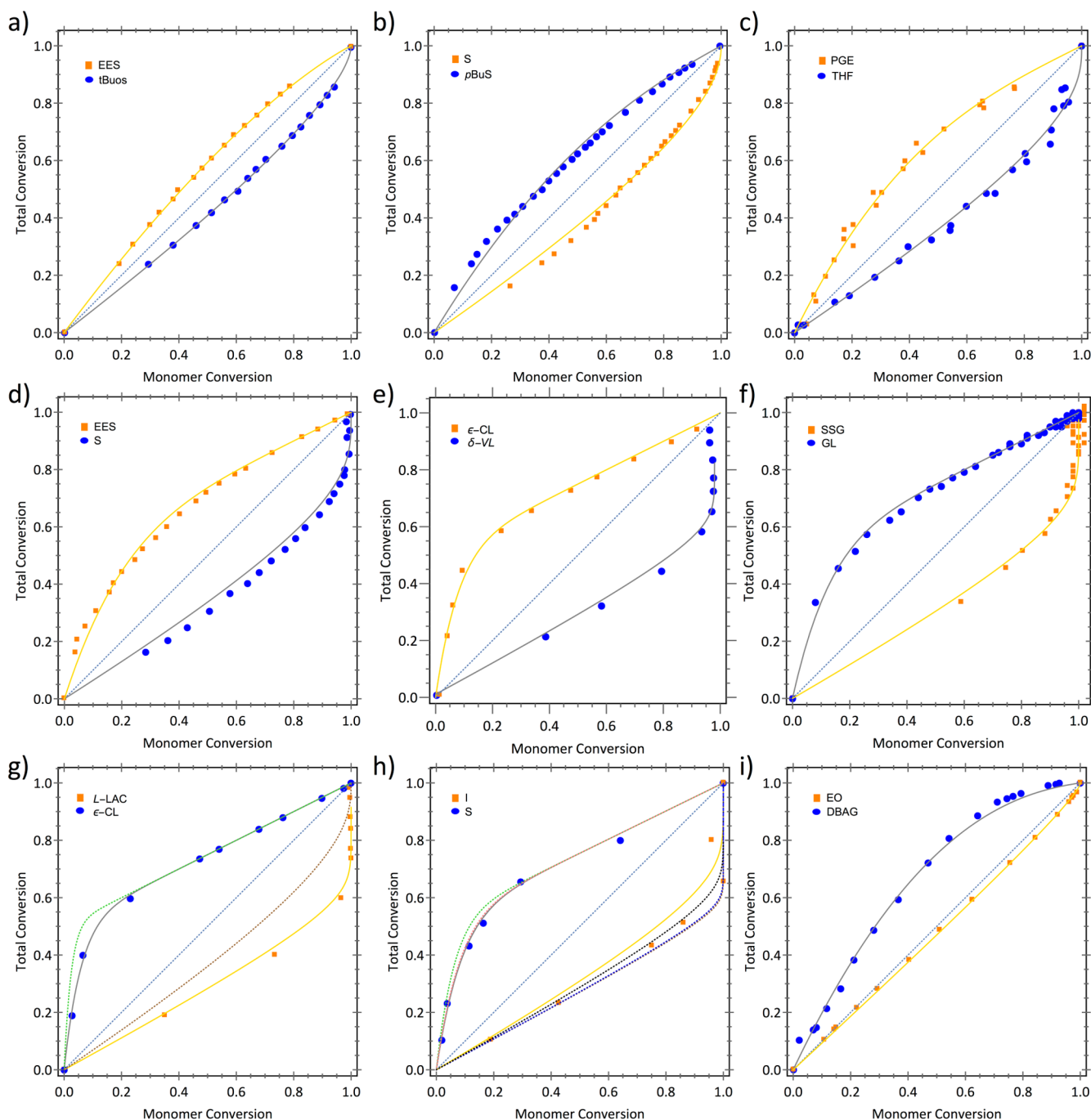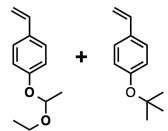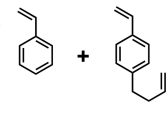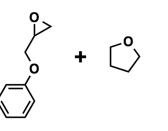
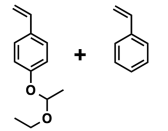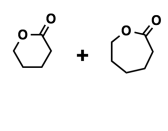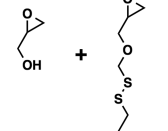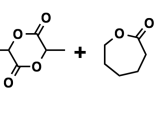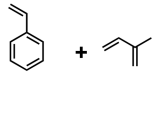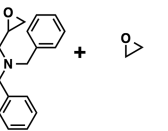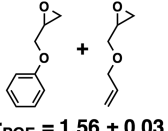**Figure 5.** Compositional drift data taken from the literature for the copolymerization of (a) (■) *p*-(1-ethoxyethoxy)styrene (EES) and (●) 4-*tert*-butoxystyrene (tBuoS),[24] (b) (■) styrene (S) and (●) *p*-but-3-enylstyrene (*p*BuS),[25] (c) (■) phenyl glycidyl ether (PGE) and (●) tetrahydrofuran (THF),[26] (d) (■) *p*-(1-ethoxyethoxy)styrene (EES) and (●) styrene (S),[24] (e) (■) *ε*-caprolactone (*ε*-CL) and (●) *δ*-valerolactone (*δ*-VL),[27] (f) (■) 2-((2-(oxiran-2-ylmethoxy)ethyl)disulfanyl)ethan-1-ol (SSG) and (●) glycerol (GL),[28] (g) (■) L-lactide (L-LAC) and (●) *ε*-caprolactone (*ε*-CL),[29] (h) (■) isoprene (I) and (●) styrene (S),[2] (i) (■) ethylene oxide (EO) and (●) *N,N*-dibenzylaminoglycidol (DBAG).[30] Dotted blue lines represent the random copolymerization case; $r_A = r_B = 1$. Solid yellow lines and gray lines represent fits to the experimental data using eqs 12 and 13. Dotted lines represent compositional drifts obtained using previously reported reactivity ratios. (g) Dotted green and dark brown lines for the values of Grijpma and Pennings.[29] (h) Dotted green and dark brown lines for the values of Worsfold[31] and dotted pink and dark blue lines for those of Quinebèche et al.[32] (h) Dotted black line represents fit using the nonterminal model using the compositional drift data for isoprene up to ~60% total conversion where 100% I conversion is reached.

two copolymerizations presented in Figure 5; L-lactide and *ε*-caprolactone shown in Figure 5g and that of styrene and isoprene presented in Figure 5h as two examples for which reactivity ratios have been previously described.

Grijpma and Penning[29] determined the reactivity ratios for L-lactide (L-LAC) and *ε*-caprolactone (*ε*-CL) using low

conversion copolymerization data obtained from ¹H NMR spectroscopy and the method of Kelen and Tüdös to obtain $r_{L\text{-LAC}} = 42$ and $r_{\varepsilon\text{-CL}} = 0.36$ whereas we obtain $r_{L\text{-LAC}} = 17.48 \pm 0.76$ and $r_{\varepsilon\text{-CL}} = 0.10 \pm 0.02$ from the nonterminal model. At first glance we note the substantial quantitative difference between the two sets of reactivity ratios both in the individual

Table 2. Reactivity Ratios Determined from Copolymerization Data Taken from the Literature[a]

(a)
$r_{EES} = 0.55 \pm 0.05$
$r_{tBuOS} = 1.68 \pm 0.01$
$r_1 r_2 = 0.92 \pm 0.08$

(b)
$r_S = 2.44 \pm 0.08$
$r_{pBuS} = 0.46 \pm 0.01$
$r_1 r_2 = 1.12 \pm 0.04$

(c)
$r_{PGE} = 0.36 \pm 0.02$
$r_{THF} = 3.07 \pm 0.13$
$r_1 r_2 = 1.11 \pm 0.08$

(d)
$r_{EES} = 0.28 \pm 0.02$
$r_S = 5.25 \pm 0.29$
$r_1 r_2 = 1.47 \pm 0.13$

(e)
$r_{\delta\text{-VL}} = 12.92 \pm 1.39$
$r_{\varepsilon\text{-CL}} = 0.10 \pm 0.01$
$r_1 r_2 = 1.29 \pm 0.19$

(f)
$r_{GL} = 8.10 \pm 0.44$
$r_{SSG} = 0.17 \pm 0.08$
$r_1 r_2 = 1.38 \pm 0.65$

(g)
$r_{L\text{-LAC}} = 17.48 \pm 0.76$
$r_{\varepsilon\text{-CL}} = 0.10 \pm 0.02$
$r_1 r_2 = 1.75 \pm 0.36$

(h)
$r_S = 0.17 \pm 0.06$
$r_I = 12.10 \pm 0.75$
$r_1 r_2 = 2.06 \pm 0.74$

(i)
$r_{DBAG} = 0.52 \pm 0.02$
$r_{EO} = 2.30 \pm 0.06$
$r_1 r_2 = 1.20 \pm 0.06$

(j)
$r_{PGE} = 1.56 \pm 0.03$
$r_{AGE} = 0.66 \pm 0.01$
$r_1 r_2 = 1.03 \pm 0.03$

[a](a) EES and tBuOS, (b) S and pBuS, (c) PGE and THF, (d) EES and S, (e) δ-VL and ε-CL, (f) GL and SSG, (g) L-LAC and ε-CL, (h) S and I, (i) DBAG and EO, and undertaken in this work: (j) PGE and AGE.

reactivity ratios, especially for $r_{L\text{-LAC}}$, and in their product (15.12 by Grijpma and Penning and 1.75 ± 0.43 here). For further comparison, we include the compositional drift curves obtained using the reactivity ratios of Grijpma and Penning in Figure 5g (shown with green and brown dotted lines) along with the fit from the nonterminal model presented here. Note how the two compositional drift curves obtained from $r_{L\text{-LAC}}$ are extremely similar, and both appear to satisfactorily overlay the monomer consumption data for ε-CL. This comparison highlights how compositional drift becomes relatively insensitive to variations as the reactivity ratios become exceedingly large and small in contrasting magnitude. In contrast, the two values of $r_{\varepsilon\text{-CL}}$ are comparatively close in absolute magnitude (0.36 vs 0.10) but produce substantially different compositional drift curves, as reflected in Figure 5g. Indeed, the value obtained here using the nonterminal model appears to more accurately represent the observed compositional drift. Because of this improved representation of the observed compositional drift, for ε-CL in particular, we find the nonterminal model better suited to describe the compositional drift for this copolymerization and that its simplicity and ease of application make it a good first model for characterizing copolymerization kinetics.

However, this simplicity comes with the caveat that it can, and will, indiscriminately fit experimental data for systems whose kinetics should instead be described with the terminal or

penultimate models and can thereby produce reactivity ratios that model the data but do not relate to the fundamental chemical reactions in the copolymerization. It is therefore important to be mindful of the polymerization mechanism of the system of interest and to, when necessary, perform additional validation. Namely, additional information detailing the statistics of monomer incorporation sequences—such as dyad or triad distribution from ^{13}C NMR spectroscopy—is necessary. Note that this caveat is also true for distinguishing between the terminal and penultimate models where compositional information alone is also insufficient.[33] One means with which to determine the validity of the nonterminal model presented here for a system of uncertain copolymerization mechanism is to obtain and fit compositional drift data for multiple initial monomer compositions. If the resulting reactivity ratios are consistent within experimental error, then the nonterminal model appropriately describes the copolymerization kinetics, whereas if the results are inconsistent further investigation with the more complex terminal or penultimate model would be necessary. Thus, while the nonterminal model is a facile method for reactivity ratio determination it cannot, without further investigation, conclude that the copolymerization mechanism for ε-CL and L-LAC proceeds with no dependence on the identity of the chain end if only a single copolymerization is performed. Also, while the product of the reactivity ratios obtained ($r_{L\text{-LAC}} \times r_{\varepsilon\text{-CL}} = 1.75 \pm 0.43$) deviates somewhat from unity, each reactivity ratio is obtained independently from the compositional drift data by minimizing the overall error. A reasonable fit can also be obtained by dictating $r_{L\text{-LAC}} \times r_{\varepsilon\text{-CL}} = 1$ (see Supporting Information for details).

Another interesting case to consider is the copolymerization of styrene and isoprene. For this copolymerization the compositional drift data presented in Figure 5h (see Supporting Information for an enlarged figure) was performed in cyclohexane at 30 °C. There are two previously reported sets of reactivity ratios for the copolymerization of styrene and isoprene performed in cyclohexane, however, at the slightly elevated temperature of 40 °C. In 1967, Worsfold[31] measured the homopolymerization and cross-polymerization rate constants present in the terminal model of copolymerization kinetics from which the reactivity ratios $r_S = 0.046$ and $r_I = 16.6$ are determined directly. Quinebèche et al.[32] took a similar approach in 2009 and determined the four terminal model reaction rates and thereby ultimately reported reactivity ratios: $r_S = 0.051$ and $r_I = 12.8$. The expected compositional drift is calculated using these two sets of previously reported reactivity ratios and is shown in Figure 5h. For our comparison of reactivity ratios here, we assume the reactivity ratios to be independent of temperature. While temperature is known to have pronounced effects (typically an Arrhenius type dependence)[14,22,32] on the four terminal-model propagation reaction rate constants themselves, the temperature dependencies are similar such that the reactivity ratios—as the ratio of reaction rate constants—are relatively insensitive to small differences (such as the 10 °C here) in polymerization temperature.

Examining the three fits for the compositional drift of styrene and isoprene in Figure 5h, all three yield compositional drifts for styrene that are well-matched to the experimental data. The situation is analogous to the above discussion for L-LAC and ε-CL where while the greatest discrepancy in magnitude lies with r_I, the observed compositional drift is relatively insensitive due to the large absolute value of the reactivity ratio. Similarly, the

compositional drift due to the much smaller r_S is more sensitive to changes in reactivity ratio. All three values are capable of capturing the compositional drift up to ~60% of isoprene conversion beyond which the compositional drifts from Worsfold and Quinebèche et al.'s r_S (being very similar in value) both begin to overestimate the conversion of isoprene while the nonterminal model presented here begins to underestimate it. Taking note of the scarcity of data and thereby the increased potential for biasing the fit from experimental error, we refit the compositional drift data for isoprene up to ~60% total conversion where 100% I conversion is first reached to yield the dotted black line and a new value of the reactivity ratio ($r_S = 0.10 \pm 0.16$). This approach gives a much better fit to the experimentally observed compositional drift and a marginally smaller reactivity ratio that is only slightly outside the original standard error and in agreement with the previously reported values. While the nonterminal model achieves an excellent fit to the experimental data and yields reactivity ratios within reasonable error of those obtained using traditional terminal model methods, the copolymerization of styrene and isoprene has been reported to have a chain end dependence.[31,32] In that sense, the agreement between the reactivity ratios obtained from the nonterminal model here and the reported utilizing the terminal model may be surprising. However, further investigation would be required to distinguish if this agreement is due to experimental coincidence or the result of a more fundamental trait of the copolymerization kinetics.

CONCLUSIONS

Here, we developed a methodology for the determination of reactivity ratios from kinetic polymerization data that span the full range of conversion. The nonterminal model should be generally valid for ionic and coordination polymerizations, especially those of monosubstituted epoxides, whose copolymerization tends toward *ideal* behavior, and we present the nonterminal model as the first method that should be utilized before more a complicated framework such as the terminal or penultimate model of copolymerization is used to interpret copolymerization reactivity. The nonterminal model is found capable of quantitatively determining the prescribed reactivity ratios for ideal copolymerizations through fitting simulated compositional drift data. Next, the nonterminal model was successfully applied to the copolymerization of AGE and PGE monitored by *in situ* ^{1}H NMR spectroscopy yielding reactivity ratios for this set of epoxides. Lastly, analysis of compositional drift data for nine copolymerizations for which compositional drift data are available in the literature was performed, and good fits to the experimental data were achieved and reactivity ratios obtained.

ASSOCIATED CONTENT

Ⓢ Supporting Information

The Supporting Information is available free of charge on the ACS Publications website at DOI: 10.1021/acs.macromol.5b01631.

> Additional ^{1}H NMR spectra; an enlarged Figure 5h; discussion on forcing ideal behavior with the nonterminal model (PDF)

AUTHOR INFORMATION

Corresponding Author

*E-mail lynd@che.utexas.edu (N.A.L.).

Notes

The authors declare no competing financial interest.

ACKNOWLEDGMENTS

REFERENCES

(1) Kuan, W.-F.; Roy, R.; Rong, L.; Hsiao, B. S.; Epps, T. H. *ACS Macro Lett.* **2012**, *1*, 519−523.

(2) Beckingham, B. S.; Register, R. A. *Macromolecules* **2011**, *44*, 4313−4319.

(3) Quinn, J. D.; Register, R. A. *J. Polym. Sci., Part B: Polym. Phys.* **2009**, *47*, 2106−2113.

(4) Obermeier, B.; Frey, H. *Bioconjugate Chem.* **2011**, *22*, 436−444.

(5) Hadjichristidis, N.; Hirao, A.; Tezuka, Y.; Du Prez, F. *Complex Macromolecular Architectures: Synthesis, Characterization, and Self-Assembly*; John Wiley & Sons: New York, 2011.

(6) Zhang, W.; Allgaier, J.; Zorn, R.; Willbold, S. *Macromolecules* **2013**, *46*, 3931−3938.

(7) Beckingham, B. S.; Burns, A. B.; Register, R. A. *Macromolecules* **2013**, *46*, 2760−2766.

(8) Bergman, J. A.; Cochran, E. W.; Heinen, J. M. *Polymer* **2014**, *55*, 4206−4215.

(9) Lee, B. F.; Wolffs, M.; Delaney, K. T.; Sprafke, J. K.; Leibfarth, F. A.; Hawker, C. J.; Lynd, N. A. *Macromolecules* **2012**, *45*, 3722−3731.

(10) Hawker, C. J.; Bosman, A. W.; Harth, E. *Chem. Rev.* **2001**, *101*, 3661−3688.

(11) Lutz, J.-F.; Ouchi, M.; Liu, D. R.; Sawamoto, M. *Science* **2013**, *341*, 1238149−1238149.

(12) Mayo, F. R.; Walling, C. *Chem. Rev.* **1950**, *46*, 191−287.

(13) Mayo, F. R.; Lewis, F. M. *J. Am. Chem. Soc.* **1944**, *66*, 1594−1601.

(14) Odian, G. *Principles of Polymerization*, 4th ed.; John Wiley & Sons, Inc.: Hoboken, NJ, 2004.

(15) Fineman, M.; Ross, S. D. *J. Polym. Sci.* **1950**, *5*, 259−262.

(16) Kelen, T.; Tudos, F. *J. Macromol. Sci., Chem.* **1975**, *9*, 1−27.

(17) Alfrey, T.; Price, C. C. *J. Polym. Sci.* **1947**, *2*, 101−106.

(18) Heatley, F.; Yu, G.-E.; Booth, C.; Blease, T. G. *Eur. Polym. J.* **1991**, *27*, 573−579.

(19) Boileau, S.; Deffieux, A.; Lassalle, D.; Menezes, F.; Vidal, B. *Tetrahedron Lett.* **1978**, *19*, 1767−1770.

(20) Pang, X.; Jing, R.; Huang, J. *Polymer* **2008**, *49*, 893−900.

(21) Lee, A.; Lundberg, P.; Klinger, D.; Lee, B. F.; Hawker, C. J.; Lynd, N. A. *Polym. Chem.* **2013**, *4*, 5735−5742.

(22) Hiemenz, P. C.; Lodge, T. P. *Polymer Chemistry*, 2nd ed.; CRC Press: Boca Raton, FL, 2007.

(23) Vandenberg, E. J. *J. Polym. Sci., Part A-1: Polym. Chem.* **1969**, *7*, 525−567.

(24) Natalello, A.; Werre, M.; Alkan, A.; Frey, H. *Macromolecules* **2013**, *46*, 8467−8471.

(25) Natalello, A.; Alkan, A.; von Tiedemann, P.; Wurm, F. R.; Frey, H. *ACS Macro Lett.* **2014**, *3*, 560−564.

(26) Asenjo-Sanz, I.; Veloso, A.; Miranda, J. I.; Alegría, A. *Macromolecules* **2015**, *48*, 1664−1672.

(27) Shin, E. J.; Brown, H. A.; Gonzalez, S.; Jeong, W.; Hedrick, J. L.; Waymouth, R. M. *Angew. Chem., Int. Ed.* **2011**, *50*, 6388−6391.

(28) Son, S.; Shin, E.; Kim, B.-S. *Macromolecules* **2015**, *48*, 600−609.

(29) Grijpma, D. W.; Pennings, A. J. *Polym. Bull.* **1991**, *25*, 335−341.

(30) Obermeier, B.; Wurm, F.; Frey, H. *Macromolecules* **2010**, *43*, 2244−2251.

(31) Worsfold, D. J. *J. Polym. Sci., Part A-1: Polym. Chem.* **1967**, *5*, 2783−2789.

(32) Quinebèche, S.; Navarro, C.; Gnanou, Y.; Fontanille, M. *Polymer* **2009**, *50*, 1351−1357.

(33) Hunley, M. T.; Sari, N.; Beers, K. L. *ACS Macro Lett.* **2013**, *2*, 375−379.